Published in final edited form as:
J Am Coll Cardiol. 2019 December 24; 74(25): 3124–3135. doi:10.1016/j.jacc.2019.10.036.

Transition of Macrophages to Fibroblast-Like Cells in Healing Myocardial Infarction

Nezam Haider, MD, PhD[a,b,*], **Lisardo Boscá, PhD**[c,d,*], **H. Reinier Zandbergen, MD, PhD**[e,*], **Jason C. Kovacic, MD, PhD**[a], **Navneet Narula, MD, PhD**[f], **Silvia González-Ramos, PhD**[c,d], **María Fernandez-Velasco, PhD**[d,g], **Sudhanshu Agrawal, SCYM(ASPC)**[h], **Marta Paz-García, MSc**[c], **Sudhir Gupta, MD, PhD**[h], **Kristine DeLeon-Pennell, PhD**[i], **Valentin Fuster, MD, PhD**[a,j], **Borja Ibañez, MD, PhD**[d,j,k], **Jagat Narula, MD, PhD**[a]

[a]Zena and Michael A. Wiener Cardiovascular Institute, Icahn School of Medicine at Mount Sinai, New York, New York

[b]Division of Vascular Surgery, University of Arizona, Tucson, Arizona [c]Instituto de Investigaciones Biomédicas Alberto Sols (CSIC-UAM), Arturo Duperier 4, Madrid, Spain [d]Centro de Investigación Biomédica en Red de Enfermedades Cardiovasculares, Melchor Fernández Almagro, Madrid, Spain [e]Department of Cardiothoracic Surgery, Amsterdam University Medical Center, Amsterdam, the Netherlands [f]Department of Pathology, New York University Langone Medical Center, New York, New York [g]Instituto de Investigación Biomédica LaPaz, Paseo de la Castellana, Madrid, Spain [h]Division of Basic and Clinical Immunology, University of California, Irvine, California [i]Division of Cardiology, Medical University of South Carolina, Ralph H. Johnson Veterans Affairs Medical Center, Charleston, South Carolina [j]Centro Nacional de Investigaciones Cardiovasculares (CNIC), Madrid, Spain [k]Instituto de Investigación Sanitaria-Fundación Jiménez Díaz, Madrid, Spain

Abstract

BACKGROUND—Macrophages and fibroblasts are 2 major cell types involved in healing after myocardial infarction (MI), contributing to myocardial remodeling and fibrosis. Post-MI fibrosis progression is characterized by a decrease in cardiac macrophage content.

OBJECTIVES—This study explores the potential of macrophages to express fibroblast genes and the direct role of these cells in post-MI cardiac fibrosis.

METHODS—Prolonged in vitro culture of human macrophages was used to evaluate the capacity to express fibroblast markers. Infiltrating cardiac macrophages was tracked in vivo after experimental MI of LysM(Cre$^{/+}$);ROSA26(EYFP$^{/+}$) transgenic mice. The expression of Yellow

ADDRESS FOR CORRESPONDENCE: Dr. Lisardo Boscá, Instituto de Investigaciones Biomédicas Alberto Sols (CSIC-UAM), Arturo Duperier 4, Madrid, Spain. lbosca@iib.uam.es. Twitter: @LubbDup, @Borjaibanez1, @CNIC_CARDIO.
*Drs. Haider, Boscá, and Zandbergen contributed equally to this work.

The authors have reported that they have no relationships relevant to the contents of this paper to disclose. Peter Libby, MD, served as Guest Associate Editor for this paper.

APPENDIX For experimental procedures and supplemental figures, please see the online version of this paper.

Fluorescent Protein (YFP) in these animals is restricted to myeloid lineage allowing the identification of macrophage-derived fibroblasts. The expression in YFP-positive cells of fibroblast markers was determined in myocardial tissue sections of hearts from these mice after MI.

RESULTS—Expression of the fibroblast markers type I collagen, prolyl-4-hydroxylase, fibroblast specific protein-1, and fibroblast activation protein was evidenced in YFP-positive cells in the heart after MI. The presence of fibroblasts after MI was evaluated in the hearts of animals after depletion of macrophages with clodronate liposomes. This macrophage depletion significantly reduced the number of $Mac3^{+}Col1A1^{+}$ cells in the heart after MI.

CONCLUSIONS—The data provide both in vitro and in vivo evidence for the ability of macrophages to transition and adopt a fibroblast-like phenotype. Therapeutic manipulation of this macrophage-fibroblast transition may hold promise for favorably modulating the fibrotic response after MI and after other cardiovascular pathological processes.

Keywords

cardiac fibroblast; fibroblast markers; infiltration; macrophage/fibroblast-like transition; myeloid tracers; myocardial infarction

Myocardial healing after myocardial infarction (MI) is accomplished by replacement fibros is in the damaged region, and interstitial fibros is takes place in the remote areas toward adverse ventricular remodeling. The collagen is produced by myofibroblasts, with infiltrating macrophages further facilitating this process (1,2). Macrophages infiltrate in large numbers at the site of injury after MI in human and in experimental animal models (3). These macrophages aid in the process of myocardial healing and assume multiple roles at different stages, depending on their origin whether in filtrating *or* resident (3,4). This involves removal of dead necrotic and apoptotic cells, regulation of fibroblast/myofibroblast function, and ultimately, wound resolution. Macrophages and fibroblasts are 2 major cell types involved in myocardium healing, and often lead to adverse myocardial remodeling and fibrosis (1,2,5).

It is well established that differentiated cells in various circumstances change their phenotype and transition into other cell types in adult tissues. For example, endothelial cells differentiate into beating cardiomyocytes when cocultured with neonatal rat cardiomyocytes or injected into the post-ischemic adult mouse heart (6). Studies have demonstrated the transdifferentiation of macrophages into endothelial cells (7,8) and conversion of preadipocytes into macrophages (9). In fibrosis of many tissues, the presence of fibroblasts derive from epithelial cells (10). Macrophages are versatile cells and respond aptly to the environmental cues of the site of their localization (3,4,11–13). We hypothesized that dynamic microenvironment changes during myocardial healing, which are conducive for fibrosis, can induce fibroblast-like phenotype in macrophages present at the site of infarct. This macrophage to fibroblast-like transition might augment cardiac fibrosis by collagen deposition.

In this study, we have explored the potential of macrophages to convert into collagen-producing fibroblast-like cells, in the absence of any other accessory cells. Because

components of the renin-angiotensin–aldosterone system exert a significant influence on cardiac, renal, and hepatic fibrosis (14), we also evaluated the effect of aldosterone, angiotensin II, and hypoxia on macrophage to fibroblast-like transition in vitro. Moreover, we looked for a similar macrophage to fibroblast differentiation in a mouse model of MI. Fibroblast classic markers, including type I collagen (COL1A1), prolyl-4-hydroxylase (P4H), fibroblast-specific protein-1 (FSP1/S100A4), fibroblast activation protein (FAP) and α-smooth muscle actin(SMA) were sought to evaluate this macrophage to fibroblast-like transition (15–17).

METHODS

For experimental procedures, please see the Online Appendix.

PERIPHERAL BLOOD-DERIVED CD14$^+$ MONO- CYTES

Monocytes were obtained from human ripheral blood buffy coats (each from 50 ml of blood from healthy donors) by Ficoll-Paque centrifugation. Subsequently, CD14$^+$ monocytes were isolated using EasySep Human CD14 Positive Selection Kit (Stemcell Technology, Cambridge, Massachusetts), according to the manufacturer's instructions. These cells were grown in RPMI 1640 medium (Mediatech, Mana Virginia) supplemented with 10% fetal bovine serum, 100 U/ml penicillin, 100 μg/ml streptomycin, and 2 mmol/l L-glutamine. Cells were incubated at 1–2 × 10^6 cells per well in 12 well tissue culture plates for 24 h 2 treated with 10 ng/ml of PMA to differentiate monocytes into macrophages. The individual monocyte-derived cultures used in these experiments were obtained from separate donors at different times.

PREPARATION OF CELL EXTRACTS

Whole-cell lysates were prepared by lysing cells in lysis buffer (10 mmol/l Tris; pH 7.5, 150 mmol/l NaCl, 1% NP-40, 200 μg/ml leupeptin, 10 μg/ml aprotinin, 1 mmol/l phenylmethylsulfonyl fluoride, 10 mmol/l 1 mmol/l Na_3VO_4, 1 mmol/l dithiothreitol). Protein concentration was measured using a Bio-Rad DC protein assay kit (Bio-Rad Laboratories, Hercules, California). Equal amounts of each protein sample for each assay (10 to 50 mg) were separated by 10% SDS-polyacrylamide gels and electroblotted to nitrocellulose membrane by Tran-Blot SD, Semi-Dry Transfer Cell (Bio-Rad). Membranes were then incubated with rabbit polyclonal COL1A1 antibody, anti-P4H-β mouse monoclonal antibody, antitenascin-C antibody, antitransgelin antibody, or antivimentin antibody and, after washing, with horseradish peroxidase-conjugated goat antimouse or antirabbit secondary antibodies. Immunoreactive bands were detected with ECL solution (GE Healthcare Life Sciences, Marlborough, Massachusetts).

MICE

LysM(Cre$^{/+}$);ROSA26(EYFP$^{/+}$) mice were used to track the fate of macrophages in an MI and heart failure model. LysM(Cre$^{/+}$);ROSA26(EYFP$^{/+}$) mic were generated by crossing the LysM-Cre mouse line (Jackson Laboratory, Bar Harbor, Maine; strain 004781) with the R26R-EYFP line (Jackson Laboratory; strain 006148). LysM-Cre mice express Cre in myeloid cells due to a targeted insertion in their endogenous M lysozyme locus. The R26R-

EYFP mouse is a Cre-dependent YFP reporter strain (R26R) produced by targeted insertion of EYFP preceded by a loxP flanked (floxed) transcriptional termination sequence (tpA) into the ROSA26 locus. The R26 allele terminates transcription prematurely, but when crossed with LysMCre mice, the Cre-mediated excision of the floxed termination sequence in myeloid cells leads to YFP expression. LysM($Cre^{/+}$);ROSA26($EYFP^{/+}$) mice are useful for myeloid cell tracking in vivo and exhibit specific and efficient expression of YFP protein in 83% to 98% mature macrophages and 100% granulocytes (18). In addition to the LysM($Cre^{/+}$);ROSA26($EYFP^{/+}$) mouse strain, 2-month-old male wild-type mice (C57BL6/J mice; Jackson Laboratory; strain 000664) were used for MI in the same way. When animals were depleted of resident macrophages, clodronate liposomes were administered 2 days prior to MI following the protocol provided by the supplier (Sigma-Aldrich, St. Louis, Missouri). When animals were treated with inhibitors of glycolysis (3PO) and glutaminase (C968), the drugs were dissolved in dimethylacetamide and administered intraperitoneally at 50 mg/kg body weight at day 1, and for 3 consecutive days after MI. Control subjects received equivalent amounts of dimethylacetamide. All animal studies were performed in accordance with the National Institutes of Health Guidelines for the Use of Laboratory Animals and were approved by the institutional and national boards for laboratory animal research.

EXPERIMENTAL MI AND HEART FAILURE IN MICE

After anesthesia with intramuscular ketamine (80 mg/kg) and xylazine (15mg/kg), mice were anesthetized with inhalation of 5% isoflurane and maintained with inhalation of 1% to 3% isoflurane. Mice were intubated and ventilation was maintained with a Harvard rodent positive-pressure respirator at a respiratory rate of 130 breaths/min. Mice were immobilized on a heating pad and subjected to left-sided thoracotomy between the third and fourth intercostal space. MI was induced by permanent ligation of the left anterior descending coronary artery (19). After opening the pericardium, ligation of LAD was made 1 mm under the left atrial appendage using a silk 7/0 suture. MI was confirmed by changes of the affected area from bright red to pale. The left thorax incision was closed with a 6.0 monocryl suture. The small pectoral muscle was moved back to its original place, and the skin was closed with 6.0 silk sutures. Sham-operated mice underwent a similar surgical 98% procedure except without ligation of the LAD (20). Functional parameters were determined by echocardiography/electrocardiography (Vevo 2100 System, VisualSonics, Toronto, Ontario, Canada). Hearts were harvested for analysis at 1 to 8 weeks post-MI. The heart rate, PR and QRS intervals (in milliseconds), E/A ratio of peak velocity of blood flow from gravity in early diastole (the E-wave) to peak velocity flow in late diastole caused by atrial contraction (the A-wave), and left ventricular ejection fraction were determined.

IMMUNOHISTOCHEMICAL ANALYSIS OF MYOCARDIAL TISSUE SECTIONS

At designated time points, hearts were harvested for histology. At each study, time point hearts were excised and washed with phosphate-buffered saline (PBS). Hearts were fixed in 4% paraformaldehyde in PBS followed by 30% sucrose and embedded in Tissue-Tek OCT compound (Sakura Finetek, Torrance, California). Myocardial serial tissue cryosections (5 to 7 μm) were prepared for immunofluorescence analysis. For immunostaining, tissue sections were rinsed in PBS, unspecific binding sites were blocked with 1% BSA in PBS for 60 min

at room temperature, and primary antibodies (1:100 prediluted in blocking solution) were applied for 1 h at room temperature. For double-labeling experiments, sections were washed 3 times with PBS and the second primary antibody was applied for 1 h at room temperature. Antigen-antibody complexes were visualized using fluorochrome (Alexa 484 and 594)—conjugated secondary antibodies (Invitrogen, Carlsbad, California) (prediluted in blocking solution). Photomicrographs were taken using a Leica DMIRE2 fluorescence microscope and Compix digital imaging software (Leica Microsystems Inc., Buffalo Grove, Illinois).

STATISTICAL ANALYSIS

Results are presented as mean ± SEM. Statistical significance was estimated with Student's *t*-test. Grubbs test was used to determine and discard outliers. Differences with values of $p < 0.05$ were considered statistically significant.

RESULTS

IN VITRO EXPRESSION OF FIBROBLAST MARKERS IN ACTIVATED HUMAN MACROPHAGES

Morphological changes during the transition of macrophages to fibroblast-like cells—Purified $CD14^+$ monocytes from peripheral blood were maintained in complete RPMI 1640 medium (Figure 1A, a and b). $CD14^+$ cells were treated with 10 nmol/l PMA to achieve entiation into macrophages. After overnight treatment with PMA, $CD14^+$ cells attached to the culture plate, increased in size, andacquiredamacrophage-like morphology (Figure 1A, c). No changes were observed in $CD14^-$ cells with identical PMA treatment (data not shown). PMA-treated $CD14^+$ cells were maintained in culture for up to 14 weeks without any further addition of PMA or growth factors; this was the endpoint of our experiment. During this period, activated macrophages assumed an elongated and spindle-shaped morphology, and tended to orient end-to-end or parallel to each other (Figure 1A, d). Similar results were obtained in PMA differentiated $CD14^+$ cells that were maintained in the presence of aldosterone or angiotensin II (Figure 1A, e and f).

Expression of fibroblast markers during the transition of macrophages to fibroblast-like cells—We evaluated the expression of known fibroblast markers FSP1/S100A4, α-SMA,P4H,and collagen I in activated macrophages by immunofluorescence staining. Figure 1B shows the expression of FSP1 in macrophages 1 to 12 weeks after activation; FSP1 was not detectable after 1-week culture (Figure 1B, a and b) but was gradually expressed. Most PMA-activated cells were $FSP1^+$ after 8 to 12 weeks (Figure 1B, e to h). The expression profile of α-SMA was similar to that of FSP1. No α-SMA protein was detected in early macrophages (Figure 1C, a and b), but this gradually increased after 8 to 12 weeks in culture (Figure 1C, e to h). P4H (a collagen modifying enzyme) was detected as early as 1 week after activation, and this expression increased moderately after that for up to 12 weeks (Figure 1D, a to h). Immunoblot analysis showed a low level of P4H protein in untreated $CD14^+$ monocytes. $COL1A1^+$-cell expression followed the FSP1 and α-SMA pattern (Figure 1E, a and b). COL1A1 expression increased gradually, and 8 to 12 weeks after activation, a large number of COL1A1-positive cells were detected in the culture (Figure 1E, e to h). Collagen quantification assay also detected secreted collagen in the

culture medium (Online Figure 1). In parallel to the differ-increase in the number of $COL1A1^+$ cells, the amount of secreted collagen also gradually increased in the culture medium over a period of 12 weeks.

Effect of aldosterone, angiotensin II, and hypoxic stress on macrophage to fibroblast-like cell transition—Aldosterone, angiotensin II, and hypoxic stress have been reported to enhance fibrosis in vivo, but had no effect on the transition of activated macrophages to fibroblast-like cells in culture. Macrophages treated with aldosterone or angiotensin II (Online Figure 2), or subjected to hypoxia alone or in combination had no effect on COL1A1 protein expression in cells nor in COL1A1 secreted into the culture medium (Online Figure 3).

TRANSITION OF MACROPHAGES TO FIBROBLAST-LIKE CELLS IN HEALING MOUSE HEART AFTER MI

Cell lineage tracking for transition of macrophages to fibroblast-like cells in LysM($Cre^{/+}$);ROSA26($EYFP^{/+}$) transgenic mice—To circumvent the overlapping of cell markers present in both macrophages and fibroblasts in vivo, we used LysM($Cre^{/+}$);ROSA26($EYFP^{/+}$) transgenic mice (18). In these animals, identification and tracking of cells derived from macrophages after MI is possible due to the permanent expression of the YFP reporter protein in macrophages or different cell types derived from these macrophages. We analyzed serial heart sections obtained after MI by immunofluorescence staining for the presence of cells expressing both YFP and fibroblast markers (FSP1, FAP, COL1A1, and α-SMA). Interestingly, COL1A1 and YFP copositive cells were present in myocardial sections obtained from 1-week post-MI hearts (Figure 2A, a to c). Although the COL1A1 staining was less intense than YFP, the number of positive cells was higher. In tissue sections from 6 weeks post-MI, clusters of YFP and intense COL1A1-stained copositive cells were present (Figure 2A, d to f). Cells expressing both FSP1 and YFP were also present in 1- and 8-week post-MI heart samples (Figure 2B). Expression of FSP1 progressively increased over a period of time after MI and fitted the reported trajectory of cardiac fibrosis. FAP was expressed in YFP-positive cells in the heart at 6 and 8 weeks post-MI (Figure 2C). A large number of cells were positive for α-SMA in 1- and 6-week post-MI heart samples; however, YFP and α-SMA copositive cells were not observed in the myocardial sections analyzed (Figure 2D). This is in contrast to in vitro results where α-SMA was expressed in macrophages after 4, 8, and 12 weeks of activation.

Macrophage depletion reduced the number of $Mac3^+$ $COL1A1^+$ cells in healing mouse heart after MI—Cardiac macrophages were evaluated for fibroblast-like cell transition after MI. Experimental groups of animals treated with clodronate liposomes (for resident macrophage depletion), C968 (glutaminase inhibitor to represses the growth and invasiveness of fibroblasts), and 3PO (PFKFB3 inhibitor targeting the glycolytic flux of proinflammatory macrophages) were compared. Hearts were processed 1 week after MI for immunostaining. Myocardial transverse sections (5 μm) were stained with anti-Mac3 (CD107b) and anticollagen type I antibodies and nuclei with 4',6-diamidino-2-phenylindole. Cells showing colocalization of both markers were counted and presented as percentage of the total number of cells/field (Figure 3A). The number of $Mac3^+COL1A1^+$ cells was

significantly reduced (4.6 ± 0.7%) after clodronate treatment versus the untreated control group (8.4 ± 1.6%). Inhibition of inflammatory macrophages with 3PO significantly reduced the number of $Mac3^{+}COL1A1^{+}$ cells (4.0 ± 0.7%) in treated groups, whereas in mice administered C968 (8.3 ± 0.7), the number of $Mac3^{+}COL1A1^{+}$ cells remain unchanged (Figure 3A). The effect of these treatments on functional cardiac parameters was determined in these animals (Figures 3B to 3E). The PR interval (ms) exhibited minimal but statistically significant values in animals depleted of macrophages after clodronate administration or treated with 3PO, suggesting a minor difference in electrical conduction was observed. Indeed, cardiac macrophages contribute to physiological atrioventricular nodal conduction (21). No differences were observed in the QRS value (Figure 3B). The ratio of peak velocity blood flow (E/A ratio), heart rate, and left ventricular ejection fraction were similar regardless the treatment of the animals, following MI (Figures 3C to 3E).

Appearance of $CD90^{+}$ $F4/80^{+}$ macrophage/ fibroblast-like cells in the healing mouse heart after MI—Cells isolated from the mouse heart after MI and sham-operated groups were analyzed by flow cytometry for the presence of macrophage/fibroblast-like cells. Isolated cells were stained with cardiomyocyte (MHC^{+})-, macrophage ($F4/80^{+}$)-, and fibroblast ($CD90^{+}$)-selective antibodies for flow cytometric analysis and quantification (Figure 4A, a to b). Infarcted hearts showed an increased number of macrophages and fibroblasts, as well as $CD90^{+}F4/80^{+}$ cells versus the sham group. The number of $F4/80^{+}$ cells in the heart increased from 5.4 ± 1.7% in sham operated to 14.9 ± 3.4% after MI, whereas the number of $CD90^{+}$ cells increased from 0.48 ± 0.41% to 3.4 ± 1.5%. Cells with both macrophage and fibroblast markers ($CD90^{+}F4/80^{+}$) were increased from 0.17 ± 0.15% to 3.5 ± 1.5% (Figure 4A, b).

Expression of macrophage and fibroblast genes in $CD/90^{+}$ $F4/80^{+}$ cells—Dual-positive $CD90^{+}F4/80^{+}$ cells were isolated by cell sorting from digested hearts from mice submitted to sham or after MI (Figure 4B, a). RNA isolated from these cells was analyzed by quantitative real-time polymerase chain reaction for the expression of macrophage and fibroblast genes (Figure 4B, b). $CD90^{+}F4/80^{+}$ cells were positive for macrophage (*Cd163, Cd68, Ly6C,* and *Csfr1*) and fibroblast (*Tagln, Vim, Ddr2,* and *Pdgfrb*) transcripts. Macrophage transcripts for *Cd163, Ly6C* were significantly up-regulated and the level of *Csfr1* was also higher in isolated $CD90^{+}F4/80^{+}$ cells post-MI versus control subjects (sham). The levels of CD163, vinculin, transgelin, and tenascin-C RNA (*Cd163, Vcl, Tagln,* and *Tnsc*) and protein levels were also significantly up-regulated in $CD90^{+}F4/80^{+}$ cells from the post-MI heart (Figure 4B, b and c). These proteins have been associated with post-MI fibroblast-induced fibrosis (22,23). However, the levels of *Ddr2* (with very low expression in these cells) and *Pdgfrb* transcripts were significantly reduced in $CD90^{+}F4/80^{+}$ cells post-MI versus control heart. Krüppel-like factor-4 (KLF4), which plays a key role in regulating phenotypic transitions of SMCs in vivo during development and after carotid ligation injury (24,25), was up-regulated in $CD90^{+}F4/80^{+}$ cells from the post-MI heart, suggesting a phenotypic transition of macrophages to fibroblast-like cells.

DISCUSSION

Transition of monocytes/macrophages into fibroblast-like cells has been reported in different pathological circumstances (i.e., renal fibrosis [13]), probably due to the plasticity of the myeloid lineage (5,26,27). In addition to this, fibroblasts in different organs during pathological remodeling show considerable phenotypic heterogeneity (28–31). This heterogeneity may be due to their different sources of origin: local tissue resident fibroblasts, progenitor cells, fibrocytes, pericytes, and EMT transition of epithelial cells (10). Therefore, the different sources of fibroblasts may dictate the outcome of wound healing and shape the degree of tissue scarring (Central Illustration). During cardiac remodeling after MI, the highly profibrotic microenvironment might induce a fibroblast-like phenotype in infiltrating macrophages, present in large numbers and contributing to healing. These fibroblast-like cells should help accomplish the ongoing process of myocardial replacement fibrosis (2,32). Several shared markers of macrophages and fibroblasts have been previously reported (33). Mouton et al. (34) identified a fibroblast-like macrophage population from the infarct region at day 7 post-MI. Similar to our findings, this macrophage population had an up-regulation of ECM genes including *Col1a1, Vlc, Tnc, Tagln,* and *Postn*. This supports the possibility that cells expressing common macrophage and fibroblast markers represent a specific cell population. To address this possible origin of fibroblasts, we tested the ability of a human macrophages to assume a fibroblast-like phenotype in vitro. In this proof of principle study, we identified an emergence of fibroblast-like cells from purified $CD14^+$ human monocytes differentiated into macrophages. Previous studies have suggested a crosstalk between macrophages and fibroblasts that may represent an additional possibility of differentiation (19,35). The notion of macrophage to fibroblast-like transition was further supported by our results in a transgenic mouse model where YFP-expressing macrophages were tracked and observed to acquire a fibroblast-like phenotype in healing MI.

Macrophages play a crucial role in cardiac fibrosis (1). First, by modulating the number and function of the fibroblasts recruited at the site of infarction, and second, more directly, by converting into fibroblast-like cells and depositing collagen and extracellular matrix. The newly converted fibroblasts did not express many fibroblast markers of a conventional fibroblast and may represent a group of pathogenic fibroblasts similar to those identified by other groups (13,15,28,29,32,36). Transcription factor KLF4 has been shown to facilitate phenotypic transition, and its up-regulation during the healing phase of mouse myocardium in $CD90^+F4/80^+$ cells indicates an ongoing macrophage to fibroblast transition (3,24,25). The newly converted pathogenic fibroblasts perhaps lack the control, competence, and finesse of a conventional fibroblast in maintaining collagen homeostasis and may engage in uncontrolled deposition of collagen and extracellular matrix. However, the possibility exists that resident macrophages in the heart can also be differentiated into fibroblast-like cells contributing to the known requirement of macrophages to improve cardiac regeneration after MI (1,3).

STUDY LIMITATIONS

The present study is intended to validate the proof-of-concept that macrophages in the heart can express characteristic fibroblast markers after MI, including the capacity to contribute to

adverse fibrosis. However, the specific role of resident versus infiltrating macrophages has not been evaluated in terms of the ability to differentiate into fibroblast-like cells. Also, the balance between the beneficial fibrosis following MI and the adverse fibrogenic effects in the course of heart healing require further in-depth analysis to determine the exact pathological contribution of the cell-transition s described in this work. Finally, the extent of the differentiation process requires quantification in terms of the percentages of cells present in the injured tissue.

Supplementary Material

Refer to Web version on PubMed Central for supplementary material.

ACKNOWLEDGMENTS

The authors thank MS. Verónica Terrón and Ms. Ana Gómez-Sáez for their valuable help in the manipulation of the animals and protein assays.

This work was supported by grants SAF2017–82436R and RTC2017–6283 from MINEICO, S2017/BMD-3686 from Comunidad de Madrid, CIVP18A3864 from Fundación Ramón Areces and CIBERCV (funded by the Instituto de Salud Carlos III), Fondos FEDER, and the Biomedical Laboratory Research and Development Service of the Veterans Affairs Office of Research and Development Award IK2BX003922 (to Dr. DeLeon-Pennell).

ABBREVIATIONS AND ACRONYMS

COL1A1	type I collagen
FAP	fibroblast activation protein
FSP1/S100A4	fibroblast-specific protein-1
MI	myocardial infarction
P4H	prolyl-4-hydroxylase
SMA	smooth muscle actin

REFERENCES

1. Cheng B, Chen HC, Chou IW, Tang TW, Hsieh PC. Harnessing the early post-injury inflammatory responses for cardiac regeneration. J Biomed Sci 2017;24:7. [PubMed: 28086885]
2. Frangogiannis NG. Inflammation in cardiac injury, repair and regeneration. Curr Opinion Cardiol 2015;30:240–5.
3. Liao X, Shen Y, Zhang R, et al. Distinct roles of resident and nonresident macrophages in nonischemic cardiomyopathy. Proc Natl Acad Sci U S A 2018;115:E4661–9. [PubMed: 29712858]
4. Bonaventura A, Montecucco F, Dallegri F. Cellular recruitment in myocardial ischaemia/reperfusion injury. Eur J Clin Invest 2016;46: 590–601. [PubMed: 27090739]
5. Laurent P, Jolivel V, Manicki P, et al. Immune-mediated repair: a matter of plasticity. Frontiers Immunol 2017;8:454.
6. Condorelli G, Borello U, De Angelis L, et al. Cardiomyocytes induce endothelial cells to transdifferentiate into cardiac muscle: implications for myocardium regeneration. Proc Natl Acad Sci U S A 2001;98:10733–8. [PubMed: 11535818]

7. Krenning G, Dankers PY, Jovanovic D, van Luyn MJ, Harmsen MC. Efficient differentiation of CD14+ monocytic cells into endothelial cells on degradable biomaterials. Biomaterials 2007;28: 1470–9. [PubMed: 17166584]
8. Rehman J, Li J, Orschell CM, March KL. Peripheral blood "endothelial progenitor cells" are derived from monocyte/macrophages and secrete angiogenic growth factors. Circulation 2003;107: 1164–9. [PubMed: 12615796]
9. Charriere G, Cousin B, Arnaud E, et al. Preadipocyte conversion to macrophage. Evidence of plasticity. J Biol Chem 2003;278: 9850–5. [PubMed: 12519759]
10. Iwano M, Plieth D, Danoff TM, Xue C, Okada H, Neilson EG. Evidence that fibroblasts derive from epithelium during tissue fibrosis. J Clin Invest 2002;110:341–50. [PubMed: 12163453]
11. Hamerman JA, Aderem A. Functional transitions in macrophages during in vivo infection with Mycobacterium bovis bacillus Calmette-Guerin. J Immunol 2001;167:2227–33. [PubMed: 11490009]
12. Strutz F, Okada H, Lo CW, et al. Identification and characterization of a fibroblast marker: FSP1. J Cell Biol 1995;130:393–405. [PubMed: 7615639]
13. Wang YY, Jiang H, Pan J, et al. Macrophage-to-myofibroblast transition contributes to interstitial fibrosis in chronic renal allograft injury. J Am Soc Nephrol 2017;28:2053–67. [PubMed: 28209809]
14. Watanabe T, Barker TA, Berk BC. Angiotensin II and the endothelium: diverse signals and effects. Hypertension 2005;45:163–9. [PubMed: 15630047]
15. Kelly T, Huang Y, Simms AE, Mazur A. Fibroblast activation protein-alpha: a key modulator of the microenvironment in multiple pathologies. Internat Rev Cell Mol Biol 2012;297:83–116.
16. Myllyharju J. Prolyl 4-hydroxylases, the key enzymes of collagen biosynthesis. Matrix Biol 2003;22:15–24. [PubMed: 12714038]
17. Rettig WJ, Garin-Chesa P, Healey JH, et al. Regulation and heteromeric structure of the fibroblast activation protein in normal and transformed cells of mesenchymal and neuroectodermal origin. Cancer Res 1993;53:3327–35. [PubMed: 8391923]
18. Abram CL, Roberge GL, Hu Y, Lowell CA. Comparative analysis of the efficiency and specificity of myeloid-Cre deleting strains using ROSA-EYFP reporter mice. J Immunol Methods 2014; 408:89–100. [PubMed: 24857755]
19. Clancy RM, Kapur RP, Molad Y, Askanase AD, Buyon JP. Immunohistologic evidence supports apoptosis, IgG deposition, and novel macrophage/ fibroblast crosstalk in the pathologic cascade leading to congenital heart block. Arthritis Rheumatism 2004;50:173–82. [PubMed: 14730614]
20. Cuadrado-Berrocal I, Gomez-Gaviro MV, Benito Y, et al. A labdane diterpene exerts ex vivo and in vivo cardioprotection against post-ischemic injury: involvement of AKT-dependent mechanisms. Biochem Pharmacol 2015;93:428–39. [PubMed: 25557296]
21. Hulsmans M, Clauss S, Xiao L, et al. Macrophages facilitate electrical conduction in the heart. Cell 2017;169:510–22.e20. [PubMed: 28431249]
22. Lighthouse JK, Small EM. Transcriptional control of cardiac fibroblast plasticity. J Mol Cell Cardiol 2016;91:52–60. [PubMed: 26721596]
23. Park WJ, Jeong D, Oh JG. Tenascin-C in cardiac hypertrophy and fibrosis: friend or foe? J Am Coll Cardiol 2017;70:1616–7. [PubMed: 28935039]
24. Ghazizadeh Z, Rassouli H, Fonoudi H, et al. Transient activation of reprogramming transcription factors using protein transduction facilitates conversion of human fibroblasts toward cardiomyocyte-like cells. Mol Biotech 2017;59: 207–20.
25. Liao X, Zhang R, Lu Y, et al. Kruppel-like factor 4 is critical for transcriptional control of cardiac mitochondrial homeostasis. J Clin Invest 2015;125: 3461–76. [PubMed: 26241060]
26. Rapino F, Robles EF, Richter-Larrea JA, et al. C/EBPalpha induces highly efficient macrophage transdifferentiation of B lymphoma and leukemia cell lines and impairs their tumorigenicity. Cell Reports 2017;19: 1281. [PubMed: 28494875]
27. Yan D, He Y, Dai J, Yang L, Wang X, Ruan Q. Vascular endothelial growth factor modified macrophages transdifferentiate into endothelial-like cells and decrease foam cell formation. Biosci Reports 2017;37.

28. Sugimoto H, Mundel TM, Kieran MW, Kalluri R. Identification of fibroblast heterogeneity in the tumor microenvironment. Cancer Biol & Therapy 2006;5:1640–6.

29. Di Carlo SE, Peduto L. The perivascular origin of pathological fibroblasts. J Clin Invest 2018;128: 54–63. [PubMed: 29293094]

30. Driskell RR, Watt FM. Understanding fibroblast heterogeneity in the skin. Trends Cell Biol 2015;25:92–9. [PubMed: 25455110]

31. Sriram G, Bigliardi PL, Bigliardi-Qi M. Fibroblast heterogeneity and its implications for engineering organotypic skin models in vitro. Eur J Cell Biol 2015;94:483–512. [PubMed: 26344860]

32. Roche PL, Filomeno KL, Bagchi RA, Czubryt MP. Intracellular signaling of cardiac fibroblasts. Comprehensive Physiol 2015;5:721–60.

33. Inoue T, Plieth D, Venkov CD, Xu C, Neilson EG. Antibodies against macrophages that overlap in specificity with fibroblasts. Kidney International 2005;67:2488–93. [PubMed: 15882296]

34. Mouton AJ, DeLeon-Pennell KY, Rivera Gonzalez OJ, et al. Mapping macrophage polarization over the myocardial infarction time continuum. Basic Res Cardiol 2018;113:26. [PubMed: 29868933]

35. Leinonen JV, Korkus-Emanuelov A, Wolf Y, et al. Macrophage precursor cells from the left atrial appendage of the heart spontaneously reprogram into a C-kit+/CD45− stem cell-like phenotype. Int J Cardiol 2016;209:296–306. [PubMed: 26913371]

36. Kim YB, Yoon YS, Choi YH, Park EM, Kang JL. Interaction of macrophages with apoptotic cells inhibits transdifferentiation and invasion of lung fibroblasts. Oncotarget 2017;8:112297–312. [PubMed: 29348826]

COMPETENCY IN MEDICAL KNOWLEDGE

In survivors of MI, transition of macrophages to fibroblasts influences the evolution of myocardial fibrosis and development of heart failure.

TRANSLATIONAL OUTLOOK

Specific targeting of pathogenic macrophage transformation to inhibit fibrosis in ways that do not interfere with normal fibroblast function may have therapeutic potential for survivors of MI.

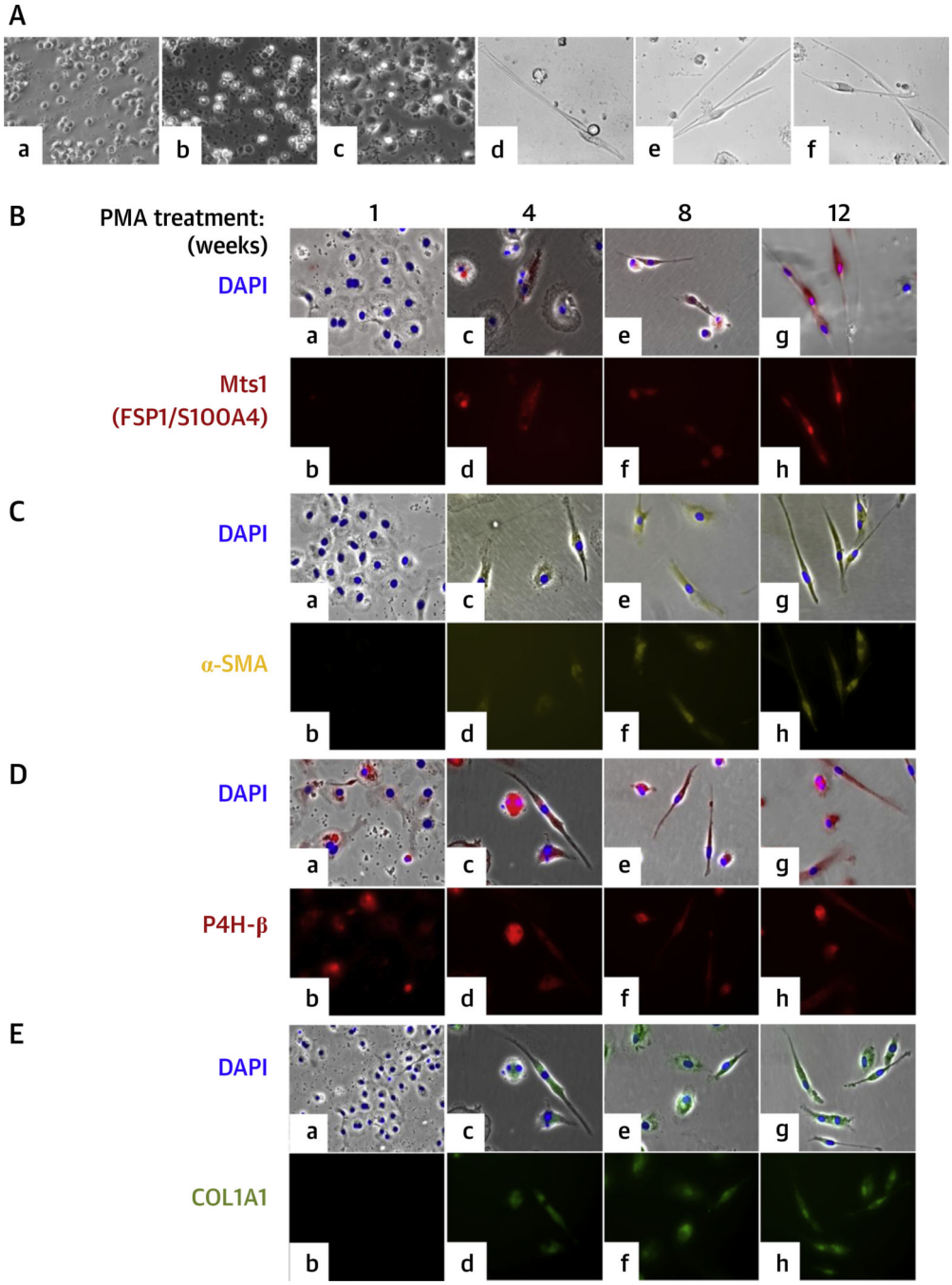

FIGURE 1. Differentiation of Human CD14$^+$ Peripheral Blood Monocytes Into Macrophages and Expression of FSP1, α-SMA, P4H-β, and COL1A1 in Macrophages Differentiated From Human CD14$^+$ Peripheral Blood Monocytes After PMA Treatment

(A) Differentiation of human CD14$^+$ peripheral blood monocytes into macrophages. **(a)** Freshly isolated monocytes. **(b)** Untreated 1-day cultured monocytes. **(c)** One-day PMA-treated monocytes. **(d)** PMA activated monocytes after 12 weeks. **(e)** PMA-activated and aldosterone-treated monocytes after 12 weeks. **(f)** PMA-activated and angiotensin II—treated monocytes after 12 weeks. Cells were visualized by phase-contrast microscopy. **(B to F)** Expression of FSP1, α-SMA, P4H-β, and COL1A1 in macrophages differentiated from

human $CD14^+$ peripheral blood monocytes after PMA treatment. Immunofluorescence staining with(B) Mts1 (FSP1/S100A4) mouse monoclonal antibody followed by Alexa Fluor 594 goat antimouse secondary antibody **(red)**; **(C)** Cy3-conjugated α-SMA antibody **(yellow); (D)** P4H-β antibody followed by Alexa Fluor 594 goat antimouse secondary antibody **(red); (E)** FITC-conjugated antihuman COL1A1 antibody **(green)** of PMA-treated cells. Nuclei were stained with 4,6-diamidino-2-phenylindole (DAPI) **(blue)**. **(a and b)** 1 week; **(c and d)** 4 weeks; **(e and f)** 8 weeks; and **(g and h)** 12 weeks after PMA activation. Cells were visualized in a Leica DMIRE2 fluorescence microscope. **(a, c, e, g)** Brightfield phase-contrast images merged with fluorescence images **(red/yellow/green)** and nuclei stained with DAPI **(blue)**. Magnification ×200. COL1A1 = type I collagen; FSP1/S100A4 = fibroblast-specific protein-1; MI = myocardial infarction; P4H = prolyl-4-hydroxylase; SMA = smooth muscle actin.

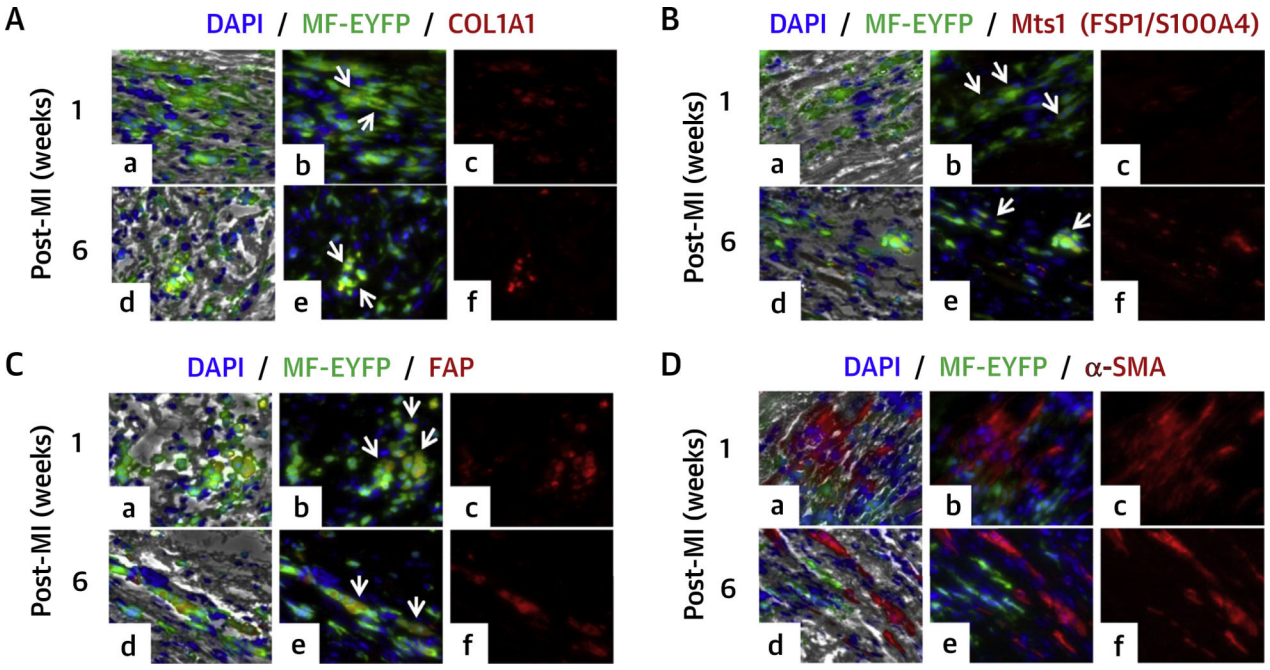

FIGURE 2. C0L1A1, FSP, FAP, and α-SMA Expression in YFP Macrophages After Myocardial Infarction in LysM(Cre$^{/+}$);ROSA26(EYFP$^{/+}$) Mouse Model

Mouse myocardial tissue sections were stained with **(A)** anti-COL1A1 antibody followed by Alexa Fluor 594 Goat secondary antibody **(red); (B)** anti-FSP1 antibody followed by Alexa Fluor 594 goat secondary antibody **(red); (C)** anti-FAP antibody followed by Alexa Fluor 594 goat secondary antibody **(red);** macrophages were stained with FITC conjugated anti-GFP antibody **(green); (D)** anti-α-SMA antibody followed by Alexa Fluor 594 goat secondary antibody **(red)**. Macrophages were stained with FITC-conjugated anti-GFP antibody **(green)**; nuclei were stained with 4,6-diamidino-2-phenylindole (DAPI) **(blue)**. **(a to c)** 1-week post-MI; **(d to f)** 6 weeks post-MI. Tissue sections were visualized under Leica DMIRE2 fluorescence microscope after staining. **(a and d)** Brightfield phase-contrast images merged with fluorescence images: COL1A, FSP1, FAP or α-SMA **(red)**, macrophages **(green)**, and nuclei **(blue); (b and e)** merged images (**red plus green; arrows** point to copositive cells **red** + **green**); **(c and f)** fluorescent image of the indicated probe **(red)**. Magnification ×200. FAP = fibroblast activation protein; other abbreviations as in Figure 1.

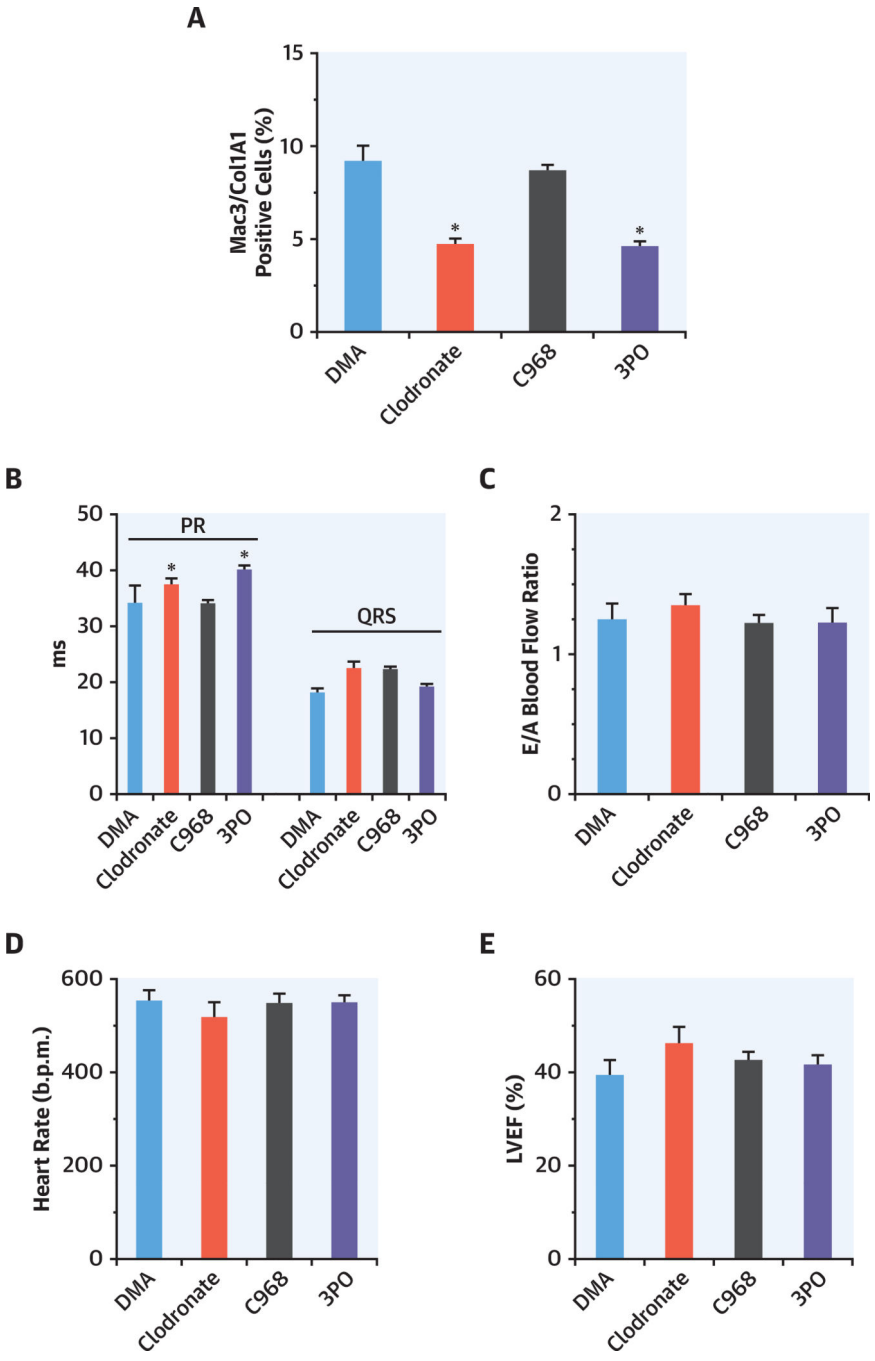

FIGURE 3. Macrophage Depletion and Inhibition of Glutaminase and PFKFB3 to Evaluate the Role of the Resident and Infiltrating Macrophages After Myocardial Infarction

Sham mice (n = 2) were treated with DMA (dimethylacetamide) (vehicle used to dissolve C968 and 3PO) for 3 consecutive days. **(A)** Animals were treated with clodronate liposomes to remove resident macrophages (n = 4; administered 1 day prior to MI); treated with the selective inhibitor of glutaminase C968 (n = 4; treated with C968 for 3 consecutive days after MI); treated with the selective inhibitor of PFKFB3 3PO that at tenuates glycolysis in proinflammatory macrophages (n = 4; treated for 3 consecutive days after MI). Hearts were processed 1 week post-MI for immunostaining. 5-μm transverse sections were stained with

anti-Mac3/CD107b and anticollagen type I secondary antibodies were Alexa Fluor 488-conjugated goat antirat and Alexa Fluor 546-conjugated goat antirabbit. Nuclei were stained with DAPI. Images were acquired with an inverted confocal microscope (Metazeiss LSM 710, Plan-Apochromat 40×/1.3 oil dic m27) and analyzed using ImageJ. **(B to E)** Functional cardiac parameters at 1 week after MI. The PR interval (ms)exhibited minimal but statistically significant higher values in animals depleted of macrophages or treated with 3PO. No differences among animal treatments after MI were observed in the QRS value, in the heart rate, in the ratio of peak velocity of blood flow (E/A ratio), and in the left ventricular ejection fraction (LVEF). *p <0.05 vs. DMA. Abbreviations as in Figure 1

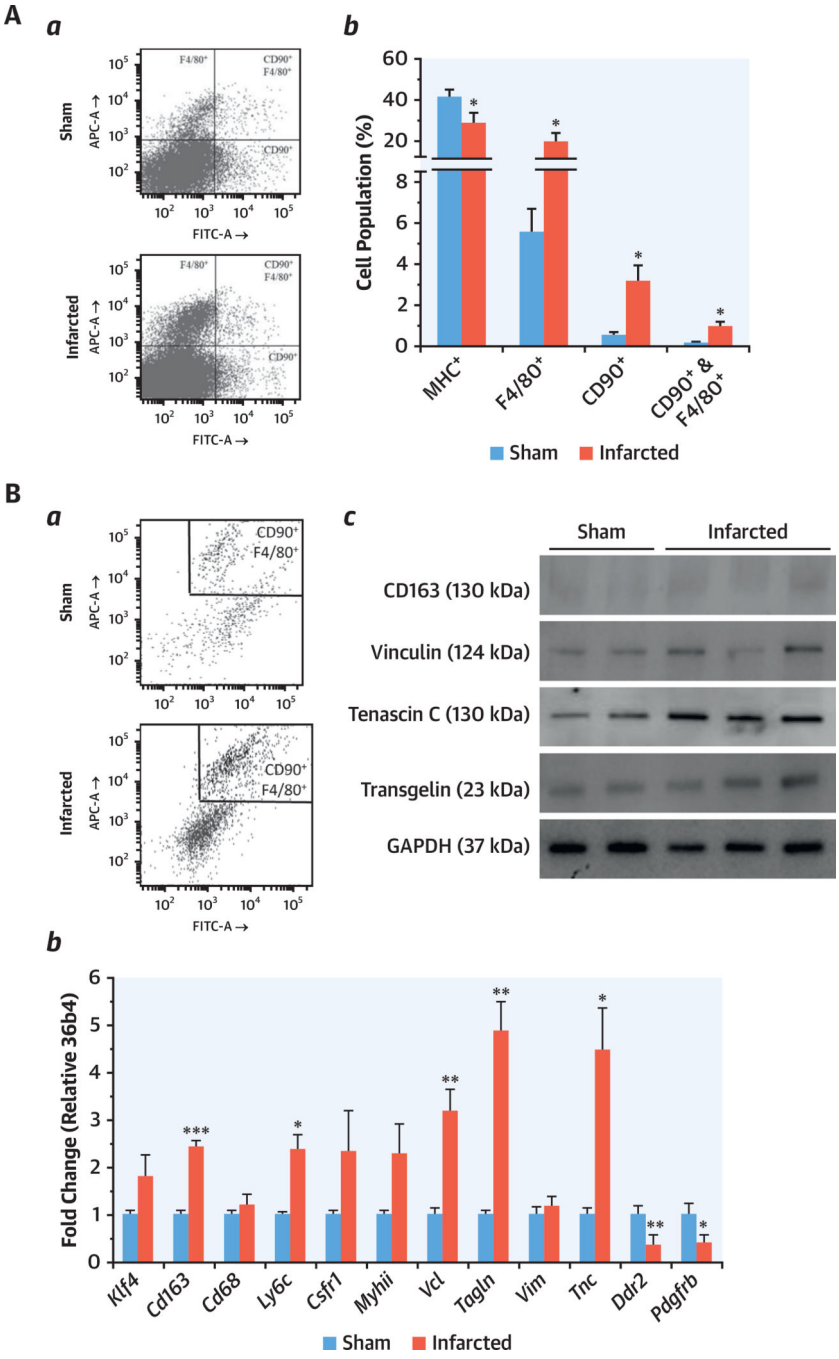

FIGURE 4. Heart-Derived Cell Populations Analysis by Flow Cytometry and Expression of Macrophage/Fibroblast Cell Markers in CD90$^+$F4/80$^+$ Cells

(A) Heart-derived cell populations analysis by flow cytometry. Sham (n = 8) and infarcted (n = 9)mice were sacrificed and, after digestion of the heart, isolated cells were labeled for CD90, F4/80, and MHC antigens. **(a)** Representative scatter plots. **(b)** The overall cell percentage for each cell population is shown. A restrictive side scatter pulse height threshold was applied in order to appreciate the minority cell populations. **(B)** Expression of macrophage/fibroblast cell markers in CD90$^+$F4/80$^+$ cells. Cells were labeled as previously

indicated, and the $CD90^{+}F4/80^{+}$ populations were sorted and aliquoted. **(a)** Representative plots of sorting. **(b)** Quantitative PCR analysis of *Klf4, Cd163, Cd68, Ly6c, Csfr1, Myhii, Vcl, Tagln, Vim, Tnc, Ddr2,* and *Pdgfrb* mRNA expression from sham and infarcted mice (n = 8 and n = 9, respectively). **(c)** Representative immunoblots of the protein levels of CD163, vinculin, transgelin, and tenascin-C of the sorted cells. mRNA amounts were normalized to m*36b4* expression (means ± SEM). Pooled samples of protein from sham of MI-sorted cells were analyzed by immunoblots (2 to 3 samples in each lane). Blots were normalized for GAPDH content. **Bars** indicate mean ± SEM. Student's *t*-test, *p < 0.05, **p < 0.005, ***p < 0.001. Abbreviations as in Figure 1.

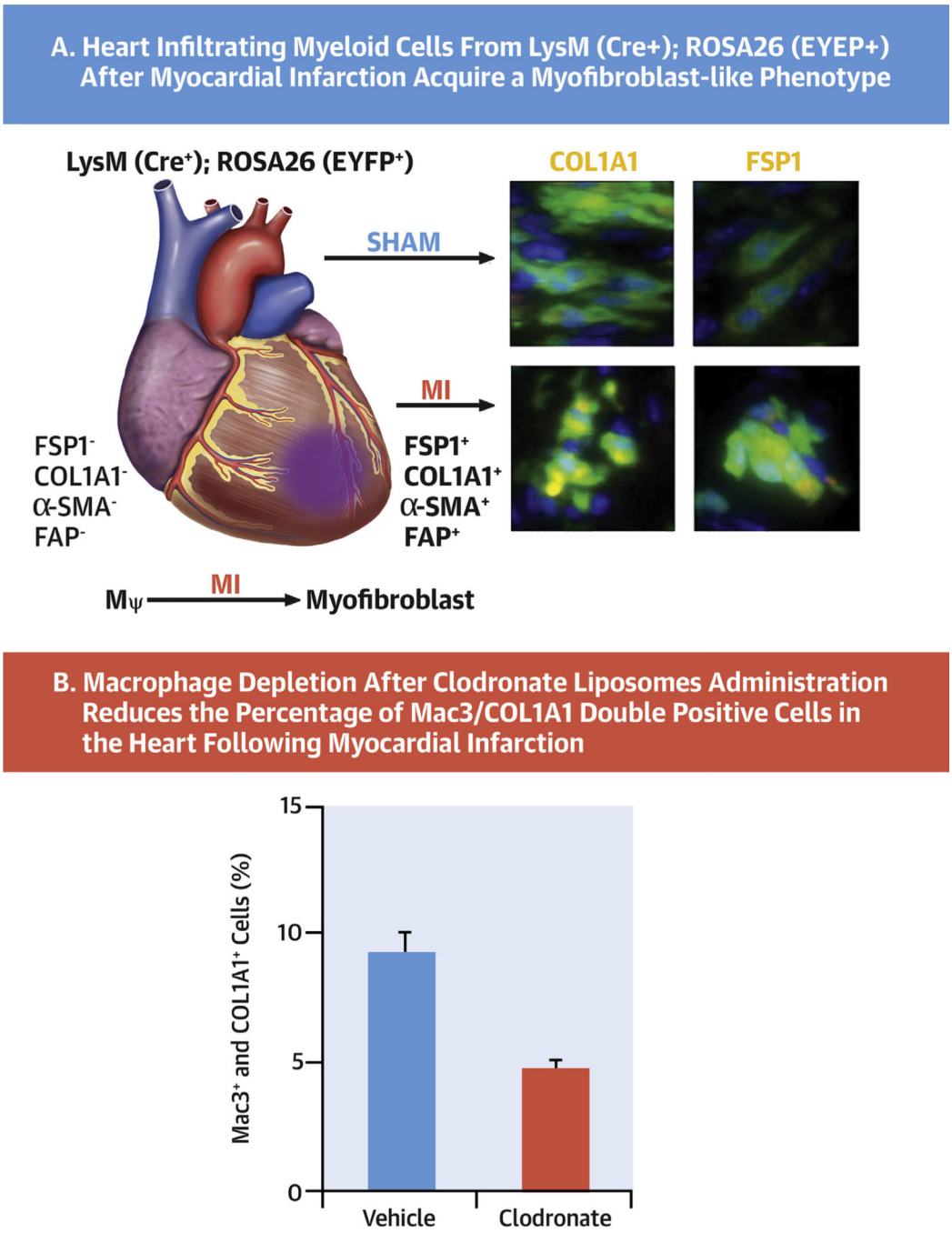

CENTRAL ILLUSTRATION. Transition of Macrophages to Fibroblast-Like Cells After Experimental Myocardial Infarction

(A) Heart infiltrating myeloid cells from LysM(Cre$^+$);ROSA26(EYFP$^+$) after myocardial infarction acquire a fibroblast-like phenotype that can be tracked with specific cell markers. **(B)** Macrophage depletion after clodronate liposomes administration reduces the percentage of Mac3/COL1A1 double-positive cells in the heart following myocardial infarction.